



# 1 Mapping 24 woody plant species phenology and ground forests 2 phenology over China from 1951-2020

3 Mengyao Zhu<sup>1</sup>, Junhu Dai<sup>1,2,3</sup>, Huanjiong Wang<sup>1</sup>, Juha M. Alatalo<sup>4</sup>, Wei Liu<sup>1,2</sup>, Yulong Hao<sup>1,2</sup>,  
4 Quansheng Ge<sup>1,2</sup>

5 <sup>1</sup>Key Laboratory of Land Surface Pattern and Simulation, Institute of Geographic Sciences and Natural Resources Research,  
6 Chinese Academy of Sciences, Beijing, 100101, China

7 <sup>2</sup>College of Resources and Environment, University of Chinese Academy of Sciences, Beijing, 101408, China

8 <sup>3</sup>China-Pakistan Joint Research Center on Earth Sciences, CAS-HEC, Islamabad, 45320, Pakistan

9 <sup>4</sup>Environmental Science Centre, Qatar University, Doha, 2713, Qatar

10 *Correspondence to:* Junhu Dai (daijh@igsnr.ac.cn); Quansheng Ge (geqs@igsnr.ac.cn)

11 **Abstract.** Plant phenology refers to the cyclic plant growth events, and is one of the most important indicators of climate  
12 change. Integration of plant phenology information is of great significance for understanding the response of ecosystems to  
13 global change and simulating the material and energy balance of terrestrial ecosystems. Based on 24552 in-situ phenology  
14 observation records of 24 typical woody plants from the Chinese Phenology Observation Network (CPON), we map the  
15 species phenology (SP) and ground phenology (GP) of forests over China from 1951-2020, with a spatial resolution of 0.1°  
16 and a temporal resolution of 1 day. A model-based upscaling method was used to generate SP maps from in-situ SP  
17 observations, and then weighted average and quantile methods were used to generate GP maps from SP maps. The validation  
18 shows that the SP maps of 24 woody plants are largely consistent with the in-situ observations, with an average error of 6.9  
19 days in spring and 10.8 days in autumn. The GP maps of forests have good agreement with the existing Land Surface  
20 Phenology (LSP) products derived by remote sensing data, particularly in deciduous forests, with an average difference of  
21 8.8 days in spring and 15.1 days in autumn. The dataset provides an independent and reliable phenology data source on a  
22 long-time scale of 70 years in China, and contributes to more comprehensive research on plant phenology and climate  
23 change at regional and national scales. The dataset can be accessed at <https://doi.org/10.57760/sciencedb.07995> (Zhu et al.,  
24 2023).

## 25 1 Introduction

26 Plant phenology refers to plant cyclic growth and development events, which are formed by adaptation to seasonal  
27 changes in climate and environmental conditions (Lieth, 1974; Schwartz, 2003). These phenological events include critical  
28 stages such as budburst, leaf unfolding, flowering, leaf coloring, and defoliation. As a highly sensitive biological indicator of  
29 climate change (Richardson et al., 2013), plant phenology is not only important for comprehending ecosystem responses to  
30 global change (Inouye, 2022; Menzel et al., 2020), but also a significant factor in simulating material and energy balance of  
31 terrestrial ecosystems (Keenan et al., 2014; Wang et al., 2020b). To be helpful for biological monitoring and predictions,



32 long-term, dependable plant phenology data on a global scale are greatly desired by related scientific research personnel.  
33 Presently, such data can be procured from diverse sources (Piao et al., 2019; Tang et al., 2016), including manual in-situ  
34 observations (Schwartz et al., 2012; Templ et al., 2018), satellite remote sensing (Bolton et al., 2020; Dixon et al., 2021), and  
35 tower-based digital cameras (Nasahara and Nagai, 2015; Richardson et al., 2018), etc. Nevertheless, integrating large-scale  
36 and long-term plant phenology information continues to pose a formidable challenge, owing to the substantial gaps in spatial  
37 and temporal scales between different data sources (Fisher et al., 2006; Park et al., 2021).

38 The practice of conducting manual, in-situ observations for species phenology (SP) boasts a rich history spanning  
39 several centuries (Aono and Kazui, 2008), yielding precise phenological information for the individual plant species (Polgar  
40 and Primack, 2011). In 1963, the Chinese Academy of Sciences inaugurated the Chinese Phenology Observation Network  
41 (CPON), a standardized, nationwide network employing a multitude of professional observers and incorporating extensive  
42 ground-based observations. To date, CPON has amassed over 1.2 million SP records pertaining to more than 900 plant  
43 species across over 150 sites throughout China (Fig. 1), cementing its dominant status as a data center for phenological  
44 research in China. These SP records have been contributed to examining the spatiotemporal patterns of plant phenological  
45 shifts (Dai et al., 2014; Ge et al., 2015), the environmental determinants influencing plant phenology (Dai et al., 2013; Wang  
46 et al., 2020a), as well as the development of phenology models in China (Tao et al., 2018; Wang et al., 2015). Nonetheless,  
47 the spatial coverage of in-situ SP data remains sporadic and restricted on regional and global scales (Donnelly et al., 2022),  
48 with noticeable gaps appearing in longer time scales. The progression of species-level phenology modeling presents an  
49 opportunity to address these limitations (Fu et al., 2020; Hufkens et al., 2018). In the absence of actual observed SP data,  
50 phenology models can be employed to generate large-scale predictions, thereby interpolating the missing SP data in both  
51 space and time (Cleland et al., 2007; Schwartz et al., 2013; Wang et al., 2012). For instance, the Extended Spring Indices  
52 (SI-x) model has been successfully applied to create gridded maps illustrating the first leaf and first bloom events for three  
53 woody plants at a resolution ranging from 1° to 1 km across the contiguous United States (Ault et al., 2015; Izquierdo-  
54 Verdiguier et al., 2018). Similarly, this model-based approach can be adapted to model and map the SP data throughout  
55 China. This would enable the integration and synthesis of CPON's long-term phenology observations at regional and  
56 national scales within the country.

57 In contrast to manual in-situ observations, satellite remote sensing facilitates the monitoring and mapping of land  
58 surface phenology (LSP) on a more expansive scale. It provides more comprehensive LSP information at the landscape level  
59 (Studer et al., 2007). Over the past four decades, remote sensing technology has witnessed considerable advancements,  
60 significantly improving the spatial and temporal resolution (Misra et al., 2020; Dronova and Taddeo, 2022). At present, a  
61 multitude of LSP products derived from vegetation indices (e.g., NDVI and EVI) procured from multi-source remote sensing  
62 data are accessible, offering regional and global LSP data with varying spatial resolutions ranging from 10 km to 30 m (e.g.,  
63 Ganguly et al., 2010; Li et al., 2019; Wu et al., 2021; Zhang et al., 2020). The credibility of these LSP data remains largely  
64 contingent upon ground phenology (GP) validation based on in-situ observed SP data (Tian et al., 2021; Zhang et al., 2017),  
65 particularly the coordination and aggregation from individual-level phenology (i.e., SP) to landscape-level phenology (i.e.,



66 GP). Weighted average and quantile methods have been proven effective for aggregating phenology from individual to  
67 community or landscape levels (Donnelly et al., 2022; Fitchett et al., 2015). Prior research has validated weighted average  
68 method on a site scale through field investigations and remote sensing monitoring, to aggregate GP at the community or  
69 landscape levels from in-situ SP data weighted by species abundance (Liang et al., 2011). Some recent studies have  
70 suggested that the quantile method (e.g., 30th percentile) holds greater promise than the commonly used average method on  
71 a larger scale, as evidenced in Europe and the USA (Ye et al., 2022). However, there is no previous study endeavored to  
72 employ these methods for aggregating large-scale GP from SP data in China, which may constrain the availability of ground  
73 validation evidence for LSP products and hinder comprehensive understanding of the spatio-temporal characteristics of  
74 phenological changes over the country.

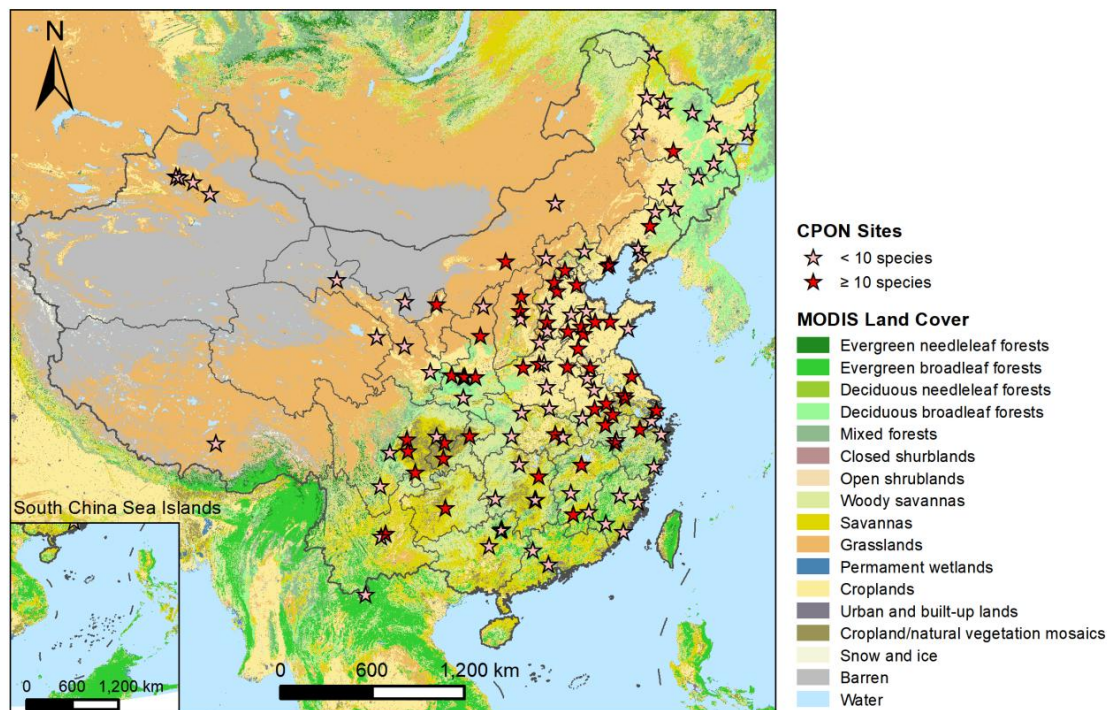
75 In this study, we aimed to develop long-term SP and GP maps of China with a  $0.1^\circ$  resolution spanning 1951-2020,  
76 supplying spatially continuous grided phenology products currently absent in the country and crucial for a wider array of  
77 applications. We utilized 24,552 in-situ phenology observations of 24 representative woody plants from 122 sites over the  
78 past six decades from CPON. Three phenophases, namely the first leaf date (FLD), first flower date (FFD), and 100% leaf  
79 coloring date (LCD), were included for each species. We employed five species-level phenology models and grided  
80 meteorological data to simulate and produce SP maps, and utilized species distribution maps as masks of SP maps for each  
81 corresponding plant species. We applied weighted average and quantile methods on SP maps to aggregate and produce GP  
82 maps, which used the distribution probabilities of each species as weights. The accuracy of SP maps was assessed through  
83 cross-validation, while the reliability of GP maps was evaluated by comparing them with existing LSP products. This study  
84 introduces a novel grid phenology dataset for China, which supplements China's existing phenology data sources and  
85 provides an independent phenology data source for LSP product verification. The dataset will facilitate more comprehensive  
86 research on plant phenology and global change by better characterizing the spatiotemporal patterns of plant phenology.

## 87 **2 Methods**

### 88 **2.1 Data acquisition and processing**

#### 89 **2.1.1 Phenology observations**

90 The in-situ phenology observations from 1963 to 2018 were obtained from the CPON. We selected 24 species of woody  
91 plants from 17 families in China (Table 1) that are common and widespread in forest ecosystems in China (Fang et al., 2011)  
92 and well-documented in CPON. These species have been observed over 55 years in 122 sites, with a total of 24,552 records,  
93 covering a range of land cover, ecological, and climatic conditions across China (Fig. 1). Each species had at least 40 years  
94 and 13 sites of phenology data. We studied three phenophases for each species: spring FLD, spring FFD, and autumn LCD.  
95 Outliers were eliminated for each species based on the principle of three sigma limits.



96  
 97 **Figure 1:** Geographic distribution of CPON sites (n = 122) included in the phenology dataset across China. Sites with less  
 98 than 10 recorded species are marked with pink asterisks, while sites with more than 10 recorded species are marked with red  
 99 asterisks. Note that the markings on the map of several adjacent sites may overlap each other. The background map shows  
 100 the IGBP land cover type from the MODIS Land Cover product (Friedl and Sulla-Menashe, 2022).

101  
 102 **Table 1:** List of 24 species of woody plants from 17 families in China. Number of records represents the total number of  
 103 three phenophases (FLD, FFD and LCD) of all sites and all years for each species.

No.	Species	Family	Life form	Number of sites	Number of years	Number of records
1	<i>Ginkgo biloba</i>	Ginkgoaceae	Tree	45	49	1110
2	<i>Metasequoia glyptostroboides</i>	Cupressaceae	Tree	37	47	860
3	<i>Magnolia denudata</i>	Magnoliaceae	Tree	42	47	980
4	<i>Salix babylonica</i>	Salicaceae	Tree	65	42	1526
5	<i>Populus × canadensis</i>	Salicaceae	Tree	43	51	954
6	<i>Robinia pseudoacacia</i>	Fabaceae	Tree	54	45	1757



7	<i>Albizia julibrissin</i>	Fabaceae	Tree	36	47	984
8	<i>Cercis chinensis</i>	Fabaceae	Shrub	52	49	1207
9	<i>Prunus armeniaca</i>	Rosaceae	Tree	46	45	950
10	<i>Ulmus pumila</i>	Ulmaceae	Tree	60	44	1428
11	<i>Morus alba</i>	Moraceae	Tree	50	50	1071
12	<i>Broussonetia papyrifera</i>	Moraceae	Tree	41	43	1103
13	<i>Quercus acutissima</i>	Fagaceae	Tree	17	40	292
14	<i>Pterocarya stenoptera</i>	Juglandaceae	Tree	29	46	936
15	<i>Juglans regia</i>	Juglandaceae	Tree	50	47	816
16	<i>Betula platyphylla</i>	Betulaceae	Tree	13	43	369
17	<i>Acer pictum</i> subsp. <i>mono</i>	Sapindaceae	Tree	18	46	492
18	<i>Ailanthus altissima</i>	Simaroubaceae	Tree	34	47	873
19	<i>Melia azedarach</i>	Meliaceae	Tree	61	46	1410
20	<i>Firmiana simplex</i>	Malvaceae	Tree	57	48	1403
21	<i>Hibiscus syriacus</i>	Malvaceae	Shrub	58	47	1096
22	<i>Fraxinus chinensis</i>	Oleaceae	Tree	23	40	505
23	<i>Syringa oblata</i>	Oleaceae	Shrub	50	51	1163
24	<i>Paulownia fortunei</i>	Paulowniaceae	Tree	49	48	1267
Total		-	-	122	55	24552

104

### 105 2.1.2 Climate data

106 The daily mean temperature (T) from 1950-2020 were obtained from two sources: (1) Site T was extracted from climate  
 107 observations in the China Meteorological Data Service Center (CMDSC, <https://data.cma.cn/>) and used to parameterize the  
 108 phenology models. (2) Grid T was extracted from ERA5-Land climate reanalysis data (Muñoz Sabater, 2019; Muñoz-  
 109 Sabater et al., 2021) from the Copernicus Climate Change Service (C3S, <https://cds.climate.copernicus.eu/>) and used for  
 110 phenology simulation and upscaling at a spatial resolution of 0.1° (about 10 km). Hourly grid T was averaged across four  
 111 phases (4:00, 10:00, 16:00, 22:00) to derive the daily grid T.

112 The current bioclimatic (BIOCLIM+) variables were obtained from Climatologies at High Resolution for the Earth  
 113 Land Surface Areas (CHELSA, <https://chelsa-climate.org/>) to determine the species distribution (Brun et al., 2022a, b). The



114 BIOCLIM+ variables indicate the average ecological and climatic conditions during 1981-2010, with a high resolution of  
115 0.0083°. We extracted the traditional 19 bioclimatic layers (Bio1-Bio19) and the complementary 50 bioclimatic layers in  
116 China. We calculated the correlation between every two layers to reduce the impact of autocorrelation among these  
117 bioclimatic layers, and then excluded the layers with a correlation coefficient greater than 0.8 with the previous layers. As a  
118 result, 12 bioclimatic layers were retained as the environmental data inputs for the species distribution models (Table S1).  
119 These layers were resampled to 0.1° to match the resolution of the grid T data.

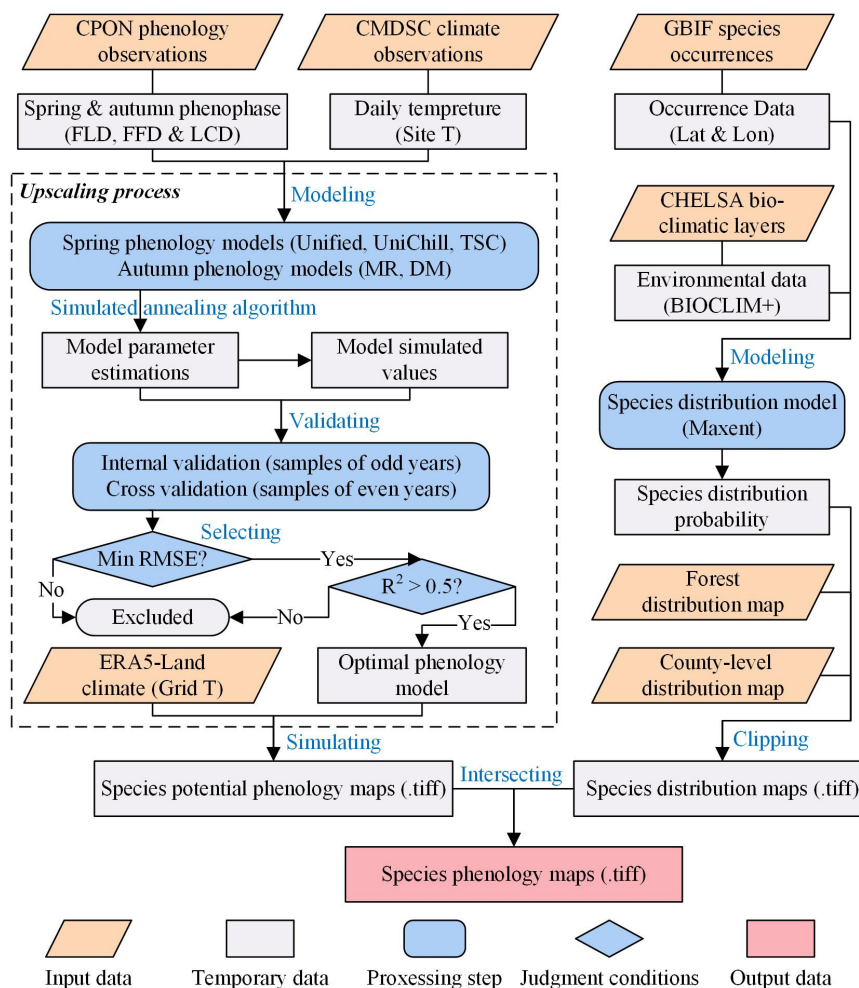
### 120 **2.1.3 Forest and species distribution data**

121 The forest distribution map of China was derived from the dataset of “Annual Dynamics of Global Land Cover and its  
122 Long-term Changes from 1982 to 2015” (Liu et al., 2020). Each year’s land cover (LC) layers were reclassified as forest and  
123 non-forest, and then the number of years of forest cover was obtained by adding all layers. Pixels with at least one year of  
124 forest cover were identified as forest distribution areas. The forest distribution map was resampled from 0.05° to 0.1° by the  
125 majority method to match the resolution of the grid T data.

126 The county-level species distribution maps were obtained from the updated Database of China's Woody Plants (Fang et  
127 al., 2011). The distribution maps in this database were compiled from all national, provincial, and regional floras and  
128 inventory reports in China published before 2009, which are considered authoritative (Cai et al., 2021). We then obtained the  
129 species occurrence records from the Global Biodiversity Information Facility (GBIF; <https://www.gbif.org/>), and used them  
130 as the occurrence data inputs for the species distribution models (GBIF, 2022). The occurrence records were filtered by  
131 including the coordinate locations with uncertainty less than 2000 meters, and cleaned by removing duplicate records.

### 132 **2.2 Generating species phenology maps using a model-based upscaling method**

133 The generation of species phenology maps involves two major processes: (1) Generating species potential phenology  
134 maps, and (2) Generating species distribution maps. The final SP maps were obtained by spatially intersecting these two  
135 maps. The workflow for the processes is shown in Fig. 2.



136

137 **Figure 2:** The workflow of generating SP maps using a model-based upscaling method, which involves two major  
 138 processes: (1) Generating species potential phenology maps, and (2) Generating species distribution maps. The words in blue  
 139 color represent the key processes of data generation. “.tiff” indicates the GeoTIFF format of the grid phenology or  
 140 distribution maps.

### 141 2.2.1 Species potential phenology maps

142 In the first process, we used a model-based upscaling method to convert in-situ phenology observations into grid  
 143 phenology maps. Phenology models were built using the phenophases (i.e., FLD, FFD, LCD) from CPON phenology  
 144 observations and the corresponding site T from CMDSC climate observations. For each species, we built three spring  
 145 phenology models: the Unichill, Unified (Chuine, 2000) and temporal-spatial coupling (TSC) models (Ge et al., 2014), and  
 146 two autumn phenology models: the multiple regression (MR) (Estrella and Menzel, 2006) and temperature-photoperiod (TP)



147 models (Delpierre et al., 2009). The details of the model formulae are described in Appendix S1. For each model, samples  
148 from odd years were used for phenology modeling, and samples from even years were reserved for cross validation on the  
149 model. All model parameters were estimated using the simulated annealing algorithm (Chuine et al., 1998).

150 For model validation, the models' root mean square error (RMSE) and goodness of fit ( $R^2$ ) were calculated between the  
151 model simulated values and original values. Internal validation was conducted on samples from odd years to evaluate the  
152 fitting effect of the model, and cross validation was conducted on samples from even years to evaluate the simulation and  
153 extrapolation effect of the model. The optimal phenology model for each species was selected based on the smallest RMSE  
154 in cross validation and  $R^2$  greater than 0.5 (0.3 for LCD) in both validations. If no model met these conditions, the species  
155 was excluded when generating SP maps or GP maps.

156 For simulating SP maps, daily grid T data from ERA5-Land climate reanalysis were input into the optimal phenology  
157 model and simulated pixel by pixel. This way, the phenology observations from individual sites were interpolated and  
158 upscaled into a grid phenology map based on the phenology models (Chuine et al., 2000). However, as long as there was  
159 grid T data, simulated species phenology could be obtained, even if there was no species distribution. Therefore, we named it  
160 as species potential phenology map to avoid taking simulated values as true values in areas without species distribution.

### 161 **2.1.2 Species distribution maps**

162 In the second process, we simulated the species distribution maps using both species distribution models and county-  
163 level species distribution data. Species distribution models were built for each species using Maximum Entropy Species  
164 Distribution Modelling (Maxent; Phillips et al., 2006) version.3.4.4. Maxent estimates the range of a species by finding the  
165 species distribution of maximum entropy (i.e., closest to the uniform), which is widely adopted in species distribution  
166 modeling (Phillips et al., 2006). It expresses a probability distribution where each grid cell has a predicted probability of  
167 presence for the species. To build the Maxent model, species location records from the GBIF database were used as  
168 occurrence data input, and the 12 bioclimatic layers from BIOCLIM+ were used as the environmental data input. In the  
169 model parameter settings, linear and quadratic feature types were used and 5-fold cross validation was used as the replicated  
170 run type.

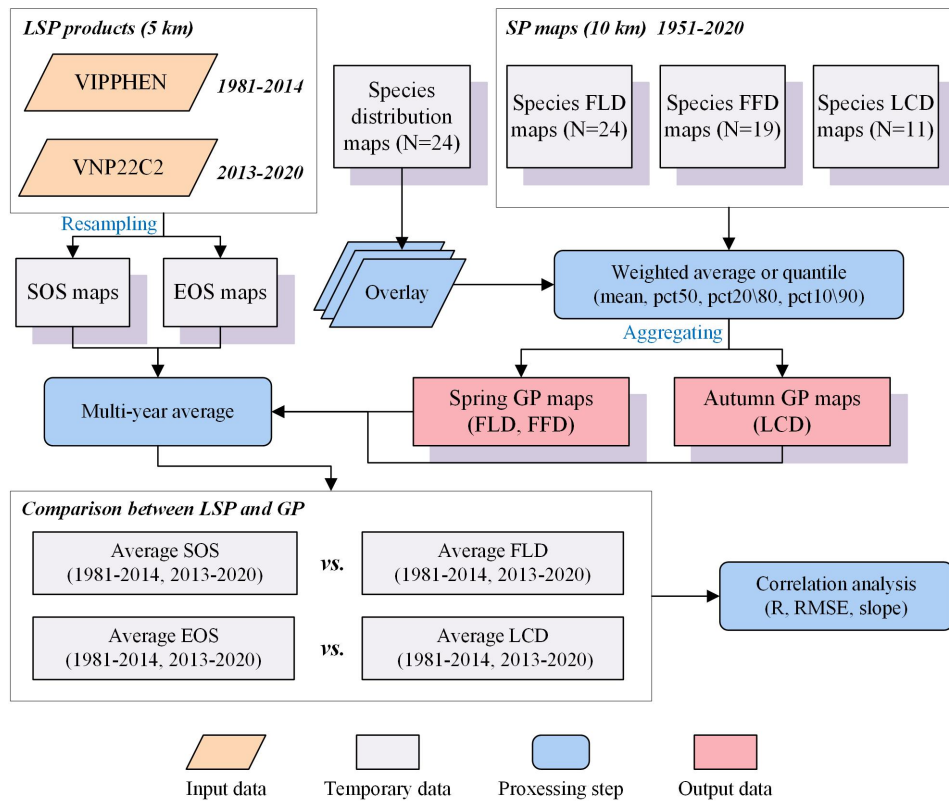
171 For model validation, the receiver operating characteristic (ROC) curve analysis method was used to test the accuracy  
172 of the Maxent prediction model. The area under the ROC curve, known as the AUC value, is usually used as an indicator of  
173 the prediction accuracy of the model (Fielding and Bell, 1997). The closer the AUC value is to 1.0, the more accurate the  
174 prediction result of the model is. The average test AUC for different species was 0.845, with a standard deviation of 0.043.

### 175 **2.3 Generating ground phenology maps using weighted average and weighted quantile methods**

176 We used four methods to aggregate from individual-level SP maps to landscape-level GP maps: (1) weighted average  
177 (mean); (2) weighted median (pct50); (3) weighted 20th percentile (pct20) for spring phenology or weighted 80th percentile  
178 (pct80) for autumn phenology; (4) weighted 10th percentile (pct10) for spring phenology or weighted 90th percentile (pct90)



179 for autumn phenology. The weight of each species was determined by the species distribution probability, as it is assumed  
 180 that the species abundance is positively related to the species distribution probability. The aggregation methods of GP in this  
 181 study (e.g., pct50, pct20\80 and pct10\90) are comparable and similar to the extraction methods of LSP from remote sensing  
 182 data (e.g., midpoint, dynamic threshold and maximum curvature). The workflow is shown in Fig. 3.  
 183



184  
 185 **Figure 3:** The workflow of generating GP maps from SP maps, and comparing GP maps with two LSP products. The words  
 186 in blue color represent the key processes of data generation.  
 187

188 For  $n$  species, the phenophases ( $Y$ ) were first sorted from small to large. The SP of each species is  $y_i$  ( $i = 1, 2, \dots, n$ ),  
 189 and the distribution probability of each species is  $p_i$  ( $i = 1, 2, \dots, n$ ). Then, the aggregated GP ( $Y_{mean}$  and  $Y_{pct}(x\%)$ ) was  
 190 calculated according to the following formulas:

191 
$$\omega_i = \frac{p_i}{\sum_{i=1}^n p_i} \quad (1)$$

192 
$$W_j = \sum_{i=1}^j \omega_i, j = 1, 2, \dots, n \quad (2)$$

193 
$$Y_{mean} = \sum_{i=1}^n \omega_i \times y_i \quad (3)$$



$$Y_{pct} = \begin{cases} y_1, & \text{if } W_1 > x \\ (y_j - y_{j-1}) \times \frac{x - W_{j-1}}{\omega_j}, & \text{if } W_j > x, W_{j-1} < x \\ y_n, & \text{if } W_{n-1} < x \end{cases} \quad (4)$$

Where  $\omega_i$  is the weight of each species,  $W_j$  is the cumulative weight from the first to the  $j$  species,  $x\%$  is the percentile tag which takes values from 10%, 20%, 50%, 80% and 90%. These formulas were used to calculate the aggregated GP maps by combining the species phenology maps with the species distribution maps and weighting them by the species distribution probability.

Finally, to assess data quality, the aggregated GP maps in this study were compared with two LSP products extracted from remote sensing in previous studies to assess data quality: (1) VIPPHEN\_NDVI product (1981-2014), which used midpoint method to extract the start of season (SOS) and the end of season (EOS) from the AVHRR data (Didan and Barreto, 2016); (2) VNP22C2 product (2013-2020), which used maximum curvature method to extract SOS and EOS from the MODIS data (Zhang et al., 2020b). Both LSP products were resampled from 5 km to  $0.1^\circ$  by the average method to match the spatial resolution of GP maps. The LSP and GP maps were averaged in two segments (1981-2014 and 2013-2020), and the correlation analysis was conducted between FLD and SOS in spring and between LCD and EOS in autumn. Pearson correlation coefficient (R), RMSE, and linear regression slope were used to evaluate the consistency between GP and LSP.

### 3 Results and discussion

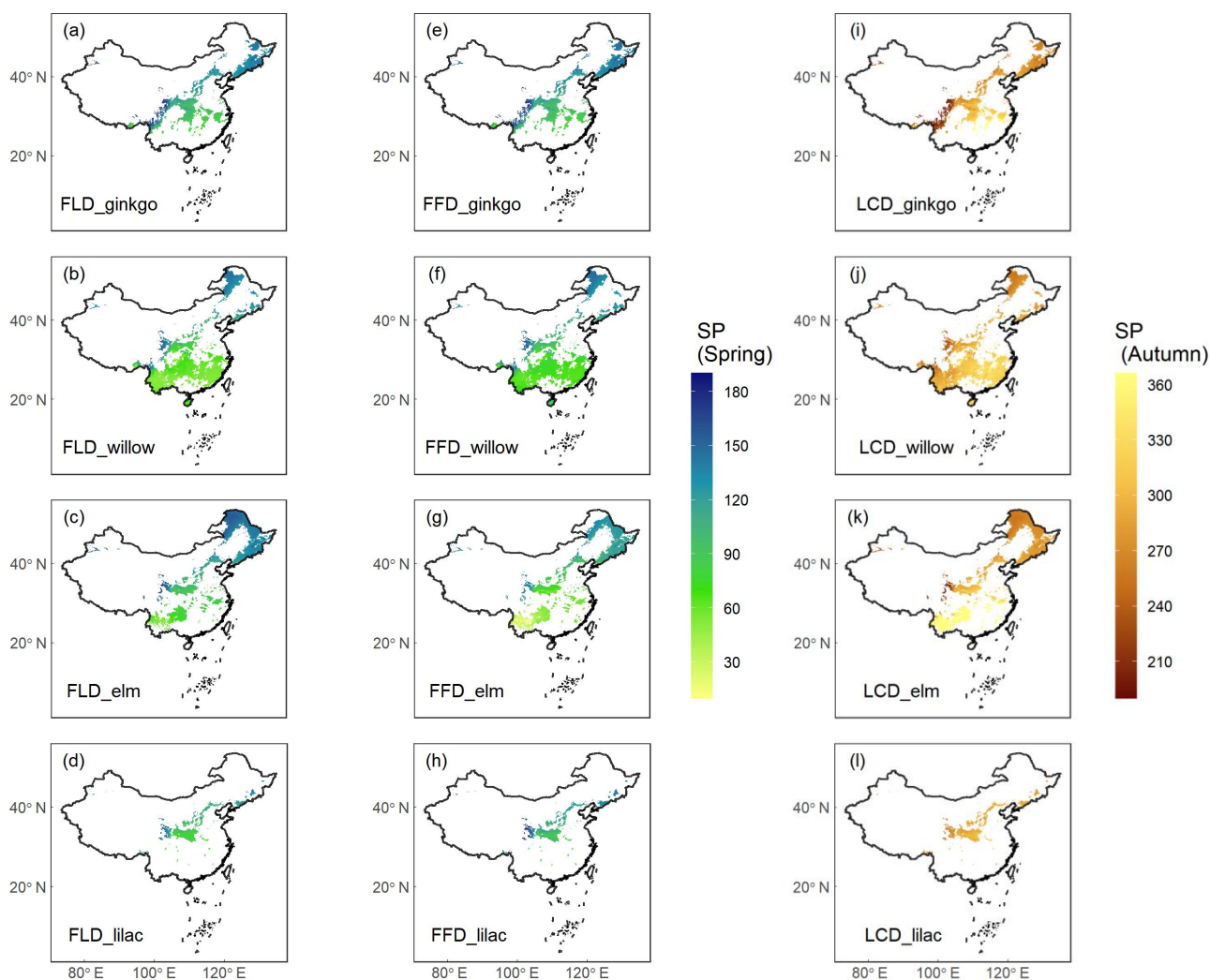
The dataset includes two types of phenology maps over China: (1) Yearly SP maps generated by the model-based upscaling method for 24 woody plants; (2) Yearly GP maps generated by four aggregation methods, along with the corresponding quality assurance (QA) maps. The phenology maps provide spring FLD, FFD, and autumn LCD of woody plants and forests over China from 1951 to 2020, with a spatial resolution of  $0.1^\circ$  and a temporal resolution of 1 day. Each map is stored in a 16-bit signed integer file in GeoTIFF format, which contains a two-dimension raster (641 row  $\times$  361 column). The unit of phenology data is the Julian Day of year (DOY), which represents the actual number of days from January 1st to the date of phenology occurrence. The valid values range from DOY 1 to 366, and the null values equal to -1.

#### 3.1 Simulation and validation of species phenology maps

The SP maps of FLD (24 species), FFD (19 species), and LCD (12 species) were simulated using the optimal phenology models, and then masked by the species distribution maps. Here, we present the results of simulated SP maps of four typical woody species (Fig. 4), including ginkgo (*Ginkgo biloba*), willow (*Salix babylonica*), elm (*Ulmus pumila*), and lilac (*Syringa oblata*). These maps showed that the phenophases of different species have a consistent spatial pattern of variation along latitude. Specifically, spring FLD and FFD of these species were significantly later with increasing latitude,



222 while autumn LCD was significantly earlier with increasing latitude. Despite similar spatial patterns, the phenophases of  
223 different species show distinct temporal differences at the same latitude; for example, at lower latitudes, elm has  
224 significantly earlier spring FFD and later autumn LCD than other species. Phenophases of some species were not simulated  
225 because the  $R^2$  of their optimal models was too small, e.g.,  $R^2 < 0.5$  for spring FFD, and  $R^2 < 0.3$  for autumn LCD.  
226



227  
228 **Figure 4:** Species phenology (SP) maps of four typical woody species averaged from 1951 to 2020. Columns 1-2 show the  
229 spring phenophases (FLD and FFD), and Column 3 shows the autumn phenophase (LCD). Each row represents a species  
230 from ginkgo (*Ginkgo biloba*), willow (*Salix babylonica*), elm (*Ulmus pumila*), and lilac (*Syringa oblata*). The unit of SP is  
231 the Julian Day of year (DOY) from January 1st.  
232



233 **Table 2:** The optimal phenology models and cross-validation results of 24 species. RMSE represents the root mean square  
 234 error between the model simulated values and original values.  $R^2$  represents goodness of fit of the optimal phenology model.

No.	Species	FLD			FFD			LCD		
		Optimal model	RMSE	$R^2$	Optimal model	RMSE	$R^2$	Optimal model	RMSE	$R^2$
1	<i>Ginkgo biloba</i>	TSC	7.30	0.669	TSC	7.53	0.553	DM	12.54	0.401
2	<i>Metasequoia glyptostroboides</i>	TSC	6.10	0.687	Unified	9.59	0.126	DM	9.99	0.295
3	<i>Magnolia denudata</i>	UniChill	6.47	0.781	TSC	7.33	0.576	DM	9.31	0.284
4	<i>Salix babylonica</i>	TSC	8.97	0.854	TSC	9.40	0.787	MR	18.23	0.380
5	<i>Populus × canadensis</i>	UniChill	5.94	0.808	UniChill	6.14	0.728	MR	9.45	0.139
6	<i>Robinia pseudoacacia</i>	TSC	5.47	0.863	TSC	6.18	0.785	DM	11.74	0.297
7	<i>Albizia julibrissin</i>	UniChill	7.48	0.500	Unified	8.23	0.376	MR	9.18	0.567
8	<i>Cercis chinensis</i>	TSC	7.90	0.723	UniChill	7.39	0.751	DM	9.09	0.175
9	<i>Prunus armeniaca</i>	TSC	6.05	0.865	UniChill	4.78	0.929	MR	14.52	0.191
10	<i>Ulmus pumila</i>	UniChill	5.09	0.901	UniChill	8.38	0.862	DM	11.16	0.654
11	<i>Morus alba</i>	TSC	6.70	0.905	UniChill	7.99	0.860	DM	9.04	0.175
12	<i>Broussonetia papyrifera</i>	UniChill	7.60	0.804	TSC	6.18	0.821	DM	9.97	0.615
13	<i>Quercus acutissima</i>	UniChill	6.73	0.931	UniChill	5.12	0.950	MR	14.35	0.765
14	<i>Pterocarya stenoptera</i>	UniChill	7.52	0.804	UniChill	7.89	0.710	MR	11.57	0.415
15	<i>Juglans regia</i>	TSC	6.04	0.739	UniChill	8.54	0.595	DM	8.41	0.141
16	<i>Betula platyphylla</i>	UniChill	3.80	0.915	UniChill	3.70	0.906	DM	8.27	0.655
17	<i>Acer pictum</i> subsp. <i>mono</i>	TSC	2.29	0.894	TSC	3.78	0.814	DM	4.71	0.670
18	<i>Ailanthus altissima</i>	UniChill	5.22	0.867	UniChill	8.34	0.664	DM	10.39	0.066
19	<i>Melia azedarach</i>	TSC	6.81	0.828	TSC	6.70	0.851	MR	10.19	0.135
20	<i>Firmiana simplex</i>	UniChill	6.02	0.694	Unified	8.10	0.314	DM	12.30	0.190
21	<i>Hibiscus syriacus</i>	TSC	9.66	0.666	Unified	13.38	0.331	DM	12.76	0.464
22	<i>Fraxinus chinensis</i>	TSC	6.25	0.852	Unified	12.35	0.319	MR	9.76	0.533
23	<i>Syringa oblata</i>	UniChill	7.01	0.864	UniChill	5.11	0.920	MR	12.36	0.475



24	<i>Paulownia fortunei</i>	UniChill	4.63	0.762	UniChill	7.02	0.693	MR	10.01	0.250
----	---------------------------	----------	------	-------	----------	------	-------	----	-------	-------

235

236

237

238

239

240

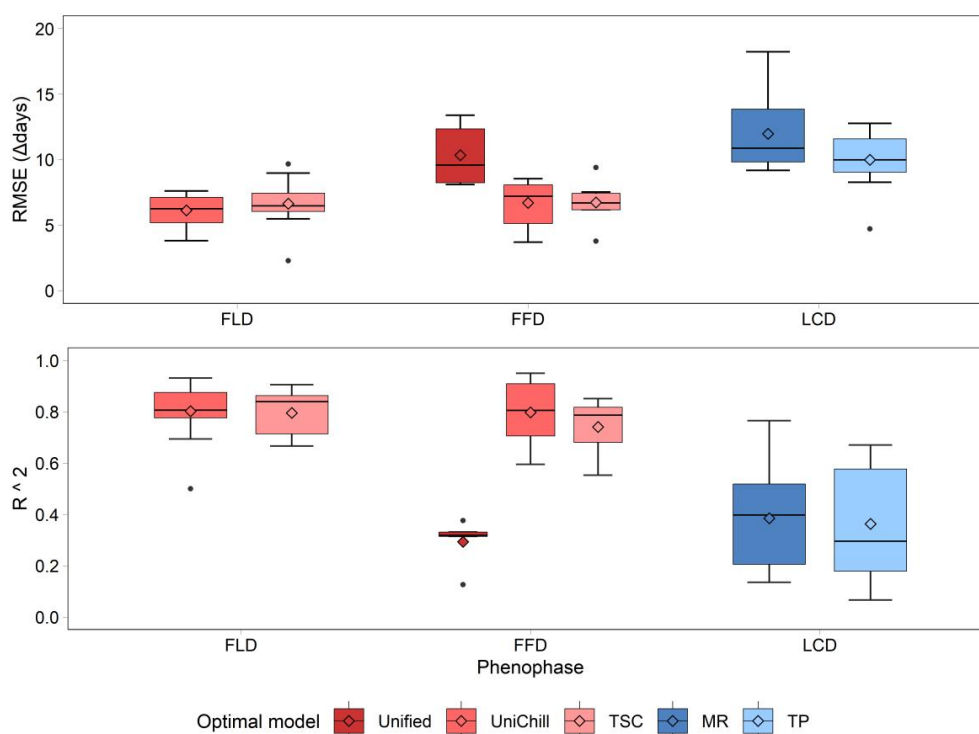
241

242

243

244

The simulation effects of species phenology maps were evaluated by cross-validation on the optimal phenology models (Table 2). The results showed that the simulation effects of spring phenology were significantly better than that of autumn phenology (Fig. 5). Specifically, the RMSE of the optimal model of FLD (6.38 days) and FFD (7.46 days) in spring were significantly smaller than that of LCD (10.80 days) in autumn. And the  $R^2$  of the optimal model of FLD (0.799) and FFD (0.676) in spring were significantly greater than that of LCD (0.372) in autumn. However, there was no significant difference between FLD and FFD simulation effects in spring. UniChill and TSC models, as the optimal model, had significantly better FFD simulation effects than Unified models for the different phenology models in spring. MR and TP models had similar LCD simulation effects for the different phenology models in autumn.



245

246

247

248

249

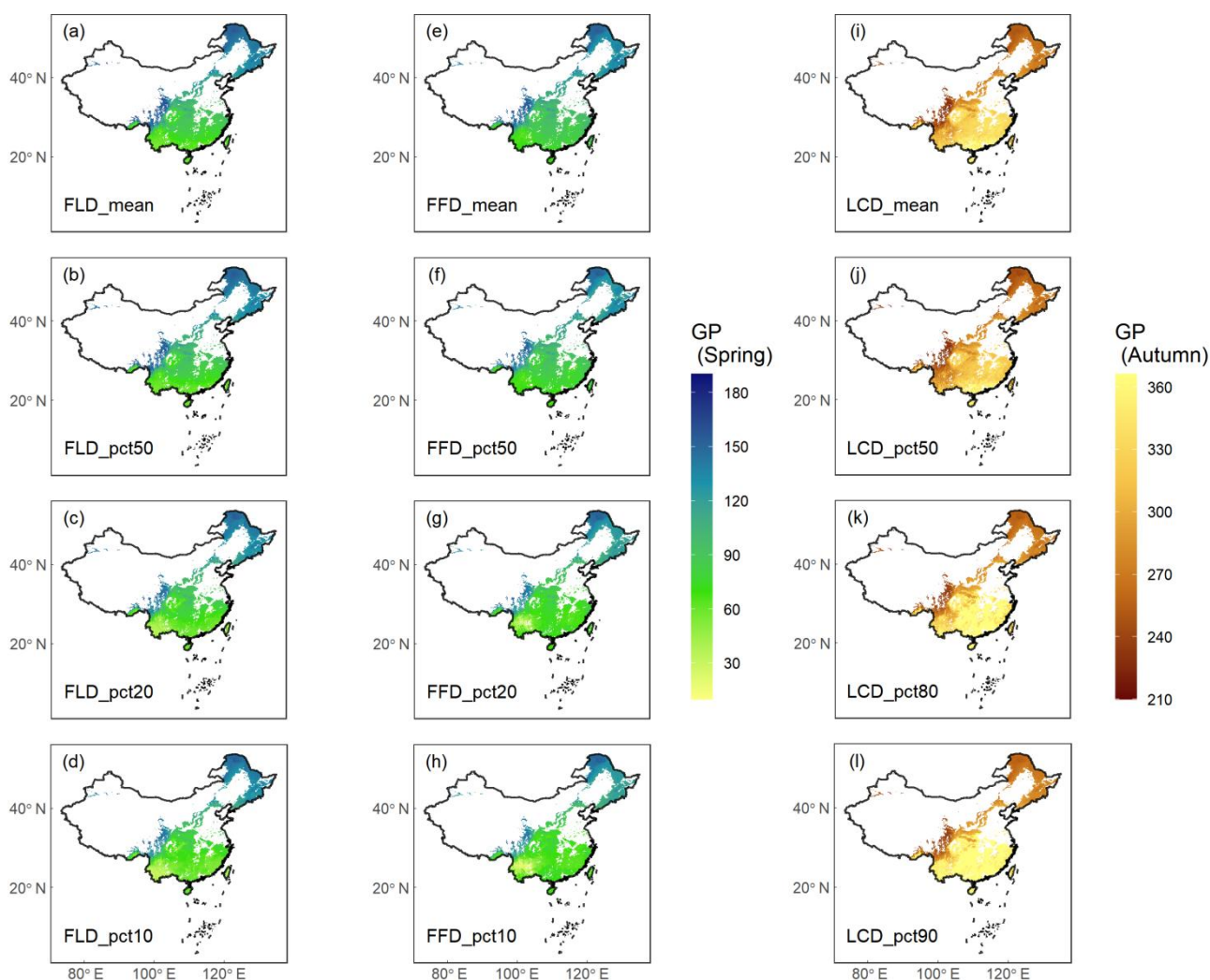
250

**Figure 5:** The RMSE (a) and  $R^2$  (b) of cross-validation on the optimal phenology models for 24 woody species. Each model is represented by a different color, with warm colors for three spring phenology models (Unified, UniChill, TSC), and cool colors for two autumn phenology models (MR, TP). The model with the smallest RMSE was selected as the optimal model for each species. The horizontal line represents the median value, the diamond mark represents the mean value, and the dot mark represents the outlier in the boxplot.



### 251 3.2 Aggregation of ground phenology maps

252 The results of GP maps generated by four different aggregation methods (mean, pct50, pct20\80, pct10\90) showed  
253 similar spatial patterns (Fig. 6), i.e., the consistent variation along latitude or altitude. With the increase of latitude or  
254 altitude, the spring GP (FLD and FFD) became later, and the autumn GP (LCD) became earlier. For different aggregation  
255 methods, the GP maps aggregated from the mean and pct50 methods were highly consistent, with R being 0.992; while the  
256 GP maps aggregated from the pct20\80 and pct10\90 methods were slightly different from the former two, with R being  
257 0.968 and 0.949, and showed larger spatial variation than the former two. The high consistency between the mean and pct50  
258 maps indicated that both the weighted mean method and weighted quantile method were robust for the aggregation of GP.  
259



260

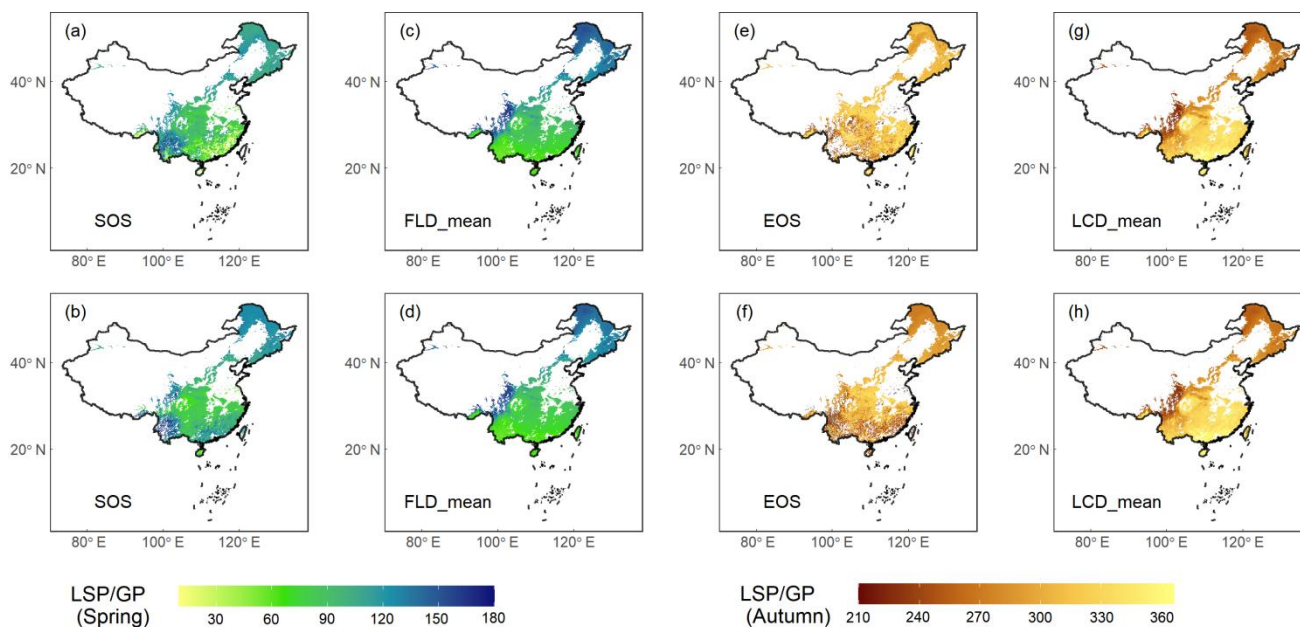


261 **Figure 6:** Ground phenology (GP) maps of four aggregation methods averaged from 1951 to 2020. Columns 1-2 show the  
262 spring phenophases (FLD and FFD), and Column 3 shows the autumn phenophase (LCD). Each row represents an  
263 aggregation method from weighted average (mean), weighted median (pct50), weighted 20% or 80% percentile (pct20\80),  
264 and weighted 10% or 90% percentile (pct10\90). The unit of GP is the Julian Day of year (DOY) from January 1st.  
265

266 We also provided two QA maps to evaluate the reliability of the aggregation results of GP maps (Fig. S1). The first is  
267 the total distribution probability of all species, and the second is the total number of species with distribution probabilities  
268 greater than 0.1. In the QA maps, higher values mean larger total number or probability of species for the aggregation,  
269 indicating that GP maps have higher reliability in these areas. The regions with the most reliable GP aggregation results were  
270 distributed around 30° N in China. The total number of species is about 15 for FLD and FFD, and is about 6 for LCD in  
271 these regions. It should be noted that in the QA map, in areas where the total number of species is less than 5 or the total  
272 probability of species is less than 1, the aggregation results of GP may not be reliable.

### 273 3.3 Data quality and usability

274 GP and LSP were compared between FLD and SOS in spring and between LCD and EOS in autumn during two  
275 segments (1981-2014 and 2013-2020). The results showed that GP and two LSP products had similar spatial patterns in  
276 central and northern China but relatively different patterns in southern China (Fig. 7), particularly for LCD and EOS in  
277 autumn (Fig. 7e-h). This is likely due to the prevalence of deciduous forests (DF) in central and northern China (Fig. 1). In  
278 contrast, evergreen forests (EF) and mixed forests (MF) are found in southern China. GP in this study was generated by  
279 aggregating the SP of 24 deciduous woody plants, which made up a large proportion of DF but a small proportion of EF or  
280 MF. Additionally, LSP extracted from remote sensing data tends to have a larger error in EF and MF due to the lack of  
281 obvious seasonal change and frequent cloud cover in these regions (Liu et al., 2016b). As a result, the consistency between  
282 GP and LSP was relatively poor in EF and MF areas (Fig. S2), with the maximum R being 0.44 in spring and 0.54 in  
283 autumn, and the minimum RMSE being 28.5 days in spring and 38.5 days in autumn (Table S2). In contrast, the consistency  
284 between GP and LSP was much better in DF area, with the maximum R being 0.95 in spring and 0.88 in autumn, and the  
285 minimum RMSE being 8.8 days in spring and 15.1 days in autumn, respectively.



286

287 **Figure 7:** Comparison of GP maps in this study and two LSP products (VIPPHEN and VNP22C2) extracted from remote  
288 sensing in previous studies, which was made between FLD and SOS in spring and LCD and EOS in autumn. Row 1 shows  
289 the comparison between VIPPHEN product and GP map averaged in 1981-2014, and Row 2 shows the comparison between  
290 VNP22C2 product and GP map averaged in 2013-2020. (a-b) SOS from two LSP products; (c-d) FLD aggregated by mean  
291 method; (e-f) EOS from two LSP products; (g-h) LCD aggregated by mean method. The unit of GP or LSP is the Julian Day  
292 of year (DOY) from January 1st.

293

294 To further assess the quality of the data, we examined the consistency between GP and LSP specifically in DF areas.  
295 The results showed that GP and LSP had good consistency in DF areas for both VIPPHEN and VNP22C2 products, i.e., high  
296 correlation (R), small difference (RMSE), and good linear relationship (Fig. 8). Compared with the LSP of VIPPHEN  
297 product, the LSP of VNP22C2 product has better consistency with the GP of this study. In addition, for both products, the  
298 consistency between GP and LSP in spring (Fig. 8e, g) was significantly better than that in autumn (Fig. 8f, h). When  
299 comparing different aggregation methods (mean, pct50, pct20/80, pct10/90), there was no significant difference in R  
300 between GP and LSP (Fig. 8a, b). All methods produced similar R values, ranging from 0.76-0.78 in spring and 0.49-0.53 in  
301 autumn for the VIPPHEN product, and from 0.90-0.91 in spring and 0.79-0.84 in autumn for the VNP22C2 product.  
302 However, different methods produced significantly different RMSE values between GP and LSP (Fig. 8c, d), largely due to  
303 the differences in the average values of GP under different methods. The best aggregation methods, with the minimum  
304 RMSE, were pct10 (20.8 days) in spring and pct90 (32.9 days) in autumn for the VIPPHEN product, and pct20 (8.8 days) in  
305 spring and pct90 (15.1 days) in autumn for the VNP22C2 product.

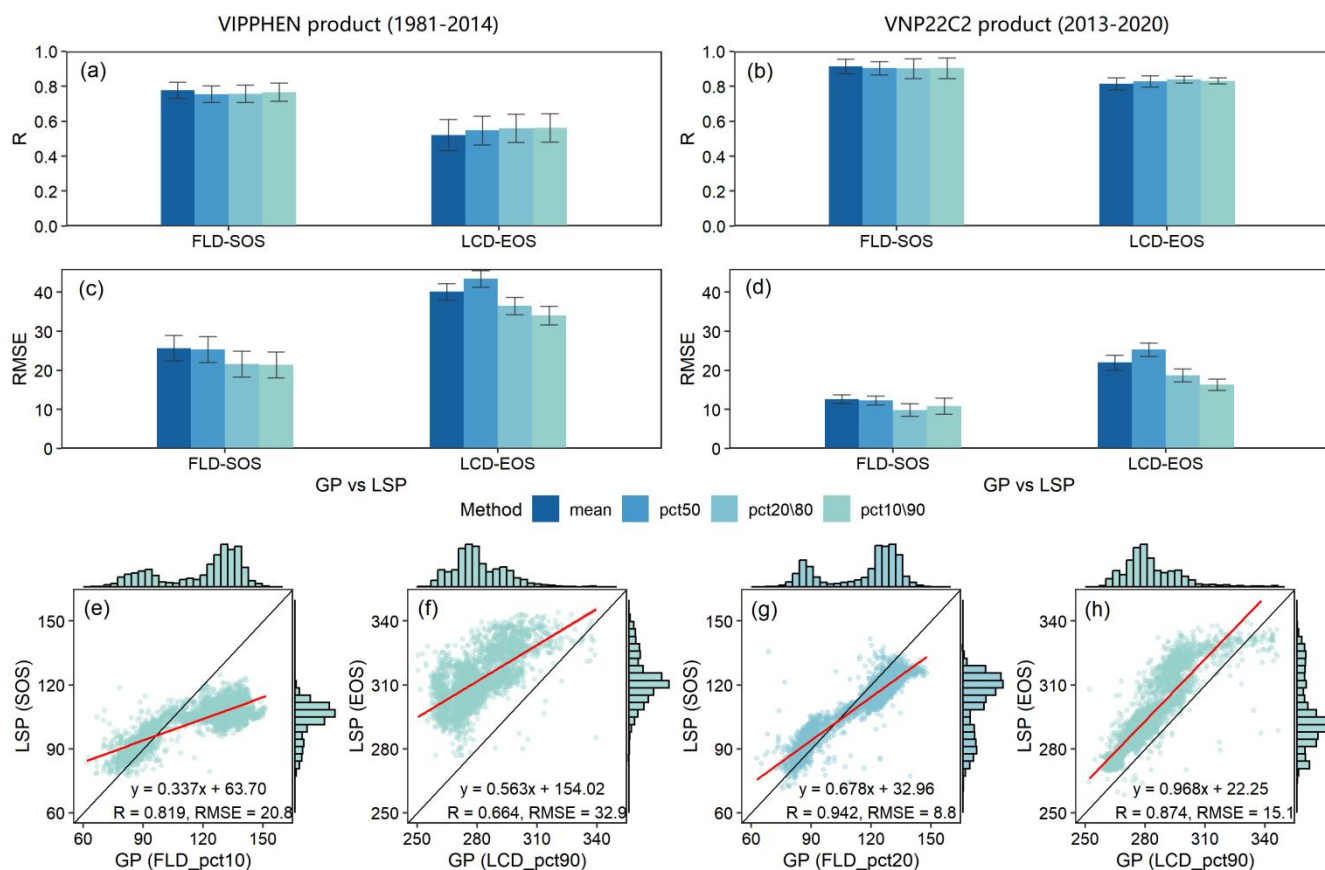


**Figure 8:** Comparison results of GP maps and two LSP products (VIPPHEN and VNP22C2) in DF areas, which was made between FLD and SOS in spring and LCD and EOS in autumn within the time range 1981-2014 and 2013-2020. (a-b) R between LSP and GP under four aggregating methods; (c-d) RMSE between LSP and GP under four aggregating methods; (e-h) Linear relationship between between LSP and GP under the best aggregating method. Each aggregating method is represented by a different color. The best aggregating method was determined by minimizing the RMSE between GP and LSP in DF areas. The error bar in the bar plot represents the multi-year standard deviation. The red line in the scatter plot represents the linear regression line between GP and LSP, and all regression results were extremely significant ( $p < 0.001$ ).

It is worth noting that the aggregation method with the smallest difference between GP and LSP in this study was the 10th or 20th percentile in spring and the 90th percentile in autumn. It means that the spring green-up event detected by remote sensing is more consistent with the FLD of earlier-developing plant species (the first 10%-20%) on the ground, while the autumn dormancy event from remote sensing is more consistent with the LCD of later-senescent plant species (the last 10%) on the ground. These results reveal a potential connection between GPs and LSPs despite their different physical implications in diagnosing phenology.



321 In general, this dataset provides high reliability SP and GP simulations of forests over China for the past 70 years. It is  
322 an independent phenology data source generated by the modeling and aggregation based on ground observations. There are  
323 several considerations in data application:

324 (1) For SP maps, the accuracy of data was determined by RMSE and  $R^2$  of cross-validation on the optimal phenology  
325 model for each species (Table 2). Additionally, the reliability of SP in space was affected by the number of sites available for  
326 modeling on each species (Table 1). For instance, the accuracy of *Betula platyphylla*'s FLD was very high overall (RMSE =  
327 3.80 and  $R^2 = 0.915$ ), but the local accuracy might be relatively poor in areas with sparse sites due to very few sites of *Betula*  
328 *platyphylla* in space ( $n = 13$ ). In this study, the SP maps of 24 species in China were found to be largely consistent with the  
329 in-situ observations, with an average error of 6.4, 7.5 and 10.8 days for FLD, FFD and LCD, respectively. These errors were  
330 the same or smaller than those of phenology modelling in previous studies. For example, the simulation error of spring FLD  
331 and FFD was 7-9 days in central Europe (Basler, 2016) and was 12.3-12.7 days in the United States (Izquierdo-Verdiguier et  
332 al., 2018), while the simulation error of autumn LCD was 10.3-13.0 days in France (Delpierre et al., 2009) and 5.9-22.8 days  
333 in the United States (Jeong and Medvigy, 2014). Therefore, compared with other studies on the regional scale, the SP maps  
334 of China in this study were found to have relatively high accuracy.

335 (2) For GP maps, the reliability of data can be determined by QA maps which provide the total number or probability of  
336 species. Additionally, the reliability can also be evaluated by comparing GP data with other LSP products, with high  
337 consistency indicating good reliability. Since GP data actually provide phenology estimates of the DF components in the  
338 forests, it has better reliability in the DF areas but less reliability in EF or MF areas. In this study, GP maps of forests in  
339 China were found have good consistency with the existing LSP products, particularly in DF areas, where the correlation  
340 coefficients of FLD and LCD were 0.91 and 0.84, respectively. The differences between GP and LSP in FLD and LCD were  
341 also found to be relatively small in DF areas, being 8.8 days and 15.1 days, respectively. Previous studies have shown poor  
342 consistency between single species and LSP, with correlation coefficients ranging from 0.50 to 0.51 in the United States  
343 (Peng et al., 2017) and Germany (Kowalski et al., 2020), and differences ranging from 12 to 14.5 days in the United States  
344 (Peng et al., 2017) and Canada (Delbart et al., 2015). In contrast, research comparing average or quantile values of multiple  
345 species has shown better results similar to this study. For example, the correlation coefficients between the average (or  
346 weighted average) GP and LSP were found to be 0.61 to 0.71 in Europe (Rodriguez-Galiano et al., 2015; Tian et al., 2021).  
347 The correlation coefficients between the 30th percentile GP and LSP were found to be 0.54 to 0.57 in China (Wu et al.,  
348 2016). The differences between the GP and LSP in previous studies were 10.3-12.4 days in China (Wu et al., 2016), 13.9  
349 days in Europe, and 12.3 days in the United States (Ye et al., 2022), which was larger than the results of FLD but smaller  
350 than that of LCD in this study. Although the landscape-level GP data aggregated from species-level SP data in this study  
351 showed good reliability, limitations in available species and different aggregation methods suggest that future comparisons  
352 between GP and LSP in other regions still need to be improved.

353 (3) For phenology maps in different seasons, the reliability of phenology data in spring was found to be significantly  
354 higher than that in autumn. The underlying reason is that the mechanism of autumn phenology is more complex compared to



355 that of spring phenology (Menzel, 2002). Moreover, the influencing factors of autumn phenology are not yet fully  
356 understood, which poses an additional challenge (Gill et al., 2015; Wu et al., 2018). In addition to temperature, other  
357 environmental factors such as precipitation (An et al., 2020), photoperiod (Lang et al., 2019), solar radiation (Wu et al.,  
358 2021b), spring phenology (Liu et al., 2016a), and growing-season productivity (Zani et al., 2020) may also drive autumn  
359 phenology. Thus, modeling autumn phenology is more challenging compared to spring phenology (Melaas et al., 2016),  
360 resulting in poorer model performance and inferior data quality of SP or GP maps in autumn.

#### 361 **4 Data availability**

362 The annual SP and GP maps over China can be accessed at <https://doi.org/10.57760/sciencedb.07995> (Zhu et al., 2023).  
363 This dataset is licensed under a CC-BY 4.0 license. The spatial reference system of the dataset is EPSG:4326(WGS84).

#### 364 **5 Conclusions**

365 In this study, mainly based on CPON historical phenology observations, we developed a new long-term gridded  
366 phenology dataset: SP maps of 24 woody plants and GP maps of forests over China from 1951–2020, with a spatial  
367 resolution of  $0.1^\circ$  and a temporal resolution of 1 day. For the generation of SP maps, we adopted a model-based upscaling  
368 method to realize the scale expansion of SP date from in-situ to regional scales in China. For the generation of GP maps, we  
369 adopted weighted average and weighted quantile methods to realize the aggregation from species to community or landscape  
370 levels in China. Dataset quality assessment shows that the average error of SP maps is 6.9 days in spring and 10.8 days in  
371 autumn, and the minimum difference between GP maps and existing LSP products is 8.8 days in spring and 15.1 days in  
372 autumn. Compared to the previous studies (Basler, 2016; Delpierre et al., 2009; Izquierdo-Verdiguier et al., 2018; Jeong and  
373 Medvigy, 2014; Tian et al., 2021; Wu et al., 2016; Ye et al., 2022), the SP maps in this study have the same or smaller  
374 simulation error, and the GP maps in this study have good agreement with other LSP products, so the data has high accuracy  
375 and reliability. This dataset is the first phenology map of China. It can be used to investigate the spatial pattern of plant  
376 phenology more clearly along the geographic gradient (e.g., longitude, latitude, and altitude), and to reveal the temporal  
377 trends (e.g., interannual, decadal, and secular) of plant phenology across China. The dataset can also provide important data  
378 support for global change impact assessment, terrestrial ecosystem simulation, and natural resource management.

#### 379 **Author contribution**

380 QG and JD designed the study and planned the modeling. HW developed the model code. WL and YH performed the  
381 simulations. MZ processed the modeling data, performed the computations and drafted the manuscript. JD and JA critically  
382 revised the manuscript. All authors discussed and contributed to the modeling and manuscript.



### 383 **Competing interests**

384 The authors declare that they have no conflict of interest.

### 385 **Acknowledgements**

386 This study was jointly supported by National Key Research and Development Program of China (2018YFA0606102),  
387 National Natural Science Foundation of China (42271062), and Strategic Priority Research Program (A) of Chinese  
388 Academy of Sciences (XDA19020303; XDA26010202). Phenology data was provided by CPON. Temperature data was  
389 provided by Copernicus Climate Change Service (C3S).

### 390 **References**

- 391 An, S., Chen, X., Zhang, X., Lang, W., Ren, S., and Xu, L.: Precipitation and minimum temperature are primary climatic  
392 controls of alpine grassland autumn phenology on the Qinghai-Tibet Plateau, *Remote Sens.*, 12, 431,  
393 <https://doi.org/10.3390/rs12030431>, 2020.
- 394 Aono, Y. and Kazui, K.: Phenological data series of cherry tree flowering in Kyoto, Japan, and its application to  
395 reconstruction of springtime temperatures since the 9th century, *Int. J. Climatol.*, 28, 905–914,  
396 <https://doi.org/10.1002/joc.1594>, 2008.
- 397 Ault, T. R., Schwartz, M. D., Zurita-Milla, R., Weltzin, J. F., and Betancourt, J. L.: Trends and natural variability of spring  
398 onset in the coterminous United States as evaluated by a new gridded dataset of spring indices, *J. Clim.*, 28, 8363–8378,  
399 <https://doi.org/10.1175/jcli-d-14-00736.1>, 2015.
- 400 Basler, D.: Evaluating phenological models for the prediction of leaf-out dates in six temperate tree species across central  
401 Europe, *Agric. For. Meteorol.*, 217, 10–21, <https://doi.org/10.1016/j.agrformet.2015.11.007>, 2016.
- 402 Bolton, D. K., Gray, J. M., Melaas, E. K., Moon, M., Eklundh, L., and Friedl, M. A.: Continental-scale land surface  
403 phenology from harmonized Landsat 8 and Sentinel-2 imagery, *Remote Sens. Environ.*, 240, 111685,  
404 <https://doi.org/10.1016/j.rse.2020.111685>, 2020.
- 405 Brun, P., Zimmermann, N., Hari, C., Pellissier, L., and Karger, D.: CHELSA-BIOCLIM+ A novel set of global climate-  
406 related predictors at kilometre-resolution, *EnviDat [data set]*, <https://doi.org/10.16904/envidat.332>, 2022a.
- 407 Brun, P., Zimmermann, N. E., Hari, C., Pellissier, L., and Karger, D. N.: Global climate-related predictors at kilometer  
408 resolution for the past and future, *Earth Syst. Sci. Data*, 14, 5573–5603, <https://doi.org/10.5194/essd-14-5573-2022>,  
409 2022b.
- 410 Cai, H., Lyu, L., Shrestha, N., Tang, Z., Su, X., Xu, X., Dimitrov, D., and Wang, Z.: Geographical patterns in phylogenetic  
411 diversity of Chinese woody plants and its application for conservation planning, *Divers. Distrib.*, 27, 179–194,  
412 <https://doi.org/10.1111/ddi.13180>, 2021.



- 413 Chuine, I.: A unified model for budburst of trees, *J. Theor. Biol.*, 207, 337–347, <https://doi.org/10.1006/jtbi.2000.2178>,  
414 2000.
- 415 Chuine, I., Cour, P., and Rousseau, D.: Fitting models predicting dates of flowering of temperate-zone trees using simulated  
416 annealing, *Plant Cell Environ.*, 21, 455–466, <https://doi.org/10.1046/j.1365-3040.1998.00299.x>, 1998.
- 417 Chuine, I., Cambon, G., and Comtois, P.: Scaling phenology from the local to the regional level: advances from species-  
418 specific phenological models, *Global Change Biol.*, 6, 943–952, <https://doi.org/10.1046/j.1365-2486.2000.00368.x>,  
419 2000.
- 420 Cleland, E. E., Chuine, I., Menzel, A., Mooney, H. A., and Schwartz, M. D.: Shifting plant phenology in response to global  
421 change, *Trends Ecol. Evol.*, 22, 357–365, <https://doi.org/10.1016/j.tree.2007.04.003>, 2007.
- 422 Dai, J., Wang, H., and Ge, Q.: Multiple phenological responses to climate change among 42 plant species in Xi'an, China,  
423 *Int. J. Biometeorol.*, 57, 749–758, <https://doi.org/10.1007/s00484-012-0602-2>, 2013.
- 424 Dai, J., Wang, H., and Ge, Q.: Characteristics of spring phenological changes in China over the past 50 years, *Adv.*  
425 *Meteorol.*, 2014, 1–8, <https://doi.org/10.1155/2014/843568>, 2014.
- 426 Delbart, N., Beaubien, E., Kergoat, L., and Le Toan, T.: Comparing land surface phenology with leafing and flowering  
427 observations from the PlantWatch citizen network, *Remote Sens. Environ.*, 160, 273–280,  
428 <https://doi.org/10.1016/j.rse.2015.01.012>, 2015.
- 429 Delpierre, N., Dufrêne, E., Soudani, K., Ulrich, E., Cecchini, S., Boé, J., and François, C.: Modelling interannual and spatial  
430 variability of leaf senescence for three deciduous tree species in France, *Agric. For. Meteorol.*, 149, 938–948,  
431 <https://doi.org/10.1016/j.agrformet.2008.11.014>, 2009.
- 432 Didan, K. and Barreto, A.: NASA MEaSUREs Vegetation Index and Phenology (VIP) Phenology NDVI Yearly Global  
433 0.05Deg CMG [Data set], NASA EOSDIS Land Processes DAAC, Accessed 2022-08-11 from  
434 [https://doi.org/10.5067/MEaSUREs/VIP/VIPPHEN\\_NDVI.004](https://doi.org/10.5067/MEaSUREs/VIP/VIPPHEN_NDVI.004), 2016.
- 435 Dixon, D. J., Callow, J. N., Duncan, J. M., Setterfield, S. A., and Pauli, N.: Satellite prediction of forest flowering  
436 phenology, *Remote Sens. Environ.*, 255, 112197, <https://doi.org/10.1016/j.rse.2020.112197>, 2021.
- 437 Donnelly, A., Yu, R., Jones, K., Belitz, M., Li, B., Duffy, K., Zhang, X., Wang, J., Seyednasrollah, B., Gerst, K. L., and  
438 others: Exploring discrepancies between in situ phenology and remotely derived phenometrics at NEON sites,  
439 *Ecosphere*, 13, e3912, <https://doi.org/10.1002/ecs2.3912>, 2022.
- 440 Dronova, I. and Taddeo, S.: Remote sensing of phenology: Towards the comprehensive indicators of plant community  
441 dynamics from species to regional scales, *J. Ecol.*, 110, 1460–1484, <https://doi.org/10.1111/1365-2745.13897>, 2022.
- 442 Estrella, N. and Menzel, A.: Responses of leaf colouring in four deciduous tree species to climate and weather in Germany,  
443 *Clim. Res.*, 32, 253–267, <https://doi.org/10.3354/cr032253>, 2006.
- 444 Fang, J., Wang, Z., and Tang, Z.: Atlas of woody plants in China: distribution and climate, Springer Science & Business  
445 Media, 2011.



- 446 Fielding, A. H. and Bell, J. F.: A review of methods for the assessment of prediction errors in conservation presence/absence  
447 models, *Environ. Conserv.*, 24, 38–49, <https://doi.org/10.1017/s0376892997000088>, 1997.
- 448 Fisher, J. I., Mustard, J. F., and Vadeboncoeur, M. A.: Green leaf phenology at Landsat resolution: Scaling from the field to  
449 the satellite, *Remote Sens. Environ.*, 100, 265–279, <https://doi.org/10.1016/j.rse.2005.10.022>, 2006.
- 450 Fitchett, J. M., Grab, S. W., and Thompson, D. I.: Plant phenology and climate change: Progress in methodological  
451 approaches and application, *Prog. Phys. Geogr.*, 39, 460–482, <https://doi.org/10.1177/0309133315578940>, 2015.
- 452 Friedl, M. and Sulla-Menashe, D.: MODIS/Terra+Aqua Land Cover Type Yearly L3 Global 500m SIN Grid V061, NASA  
453 EOSDIS Land Processes DAAC, <https://doi.org/10.5067/MODIS/MCD12Q1.061>, 2022.
- 454 Fu, Y., Li, X., Zhou, X., Geng, X., Guo, Y., and Zhang, Y.: Progress in plant phenology modeling under global climate  
455 change, *Sci. China Earth Sci.*, 63, 1237–1247, <https://doi.org/10.1007/s11430-019-9622-2>, 2020.
- 456 Ganguly, S., Friedl, M. A., Tan, B., Zhang, X., and Verma, M.: Land surface phenology from MODIS: Characterization of  
457 the Collection 5 global land cover dynamics product, *Remote Sens. Environ.*, 114, 1805–1816,  
458 <https://doi.org/10.1016/j.rse.2010.04.005>, 2010.
- 459 GBIF: GBIF Occurrence Download, GBIF.org [data set], <https://doi.org/10.15468/dl.7dwjev>, 2022.
- 460 Ge, Q., Wang, H., and Dai, J.: Simulating changes in the leaf unfolding time of 20 plant species in China over the twenty-  
461 first century, *Int. J. Biometeorol.*, 58, 473–484, <https://doi.org/10.1007/s00484-013-0671-x>, 2014.
- 462 Ge, Q., Wang, H., Rutishauser, T., and Dai, J.: Phenological response to climate change in China: a meta-analysis, *Global  
463 Change Biol.*, 21, 265–274, <https://doi.org/10.1111/gcb.12648>, 2015.
- 464 Gill, A. L., Gallinat, A. S., Sanders-DeMott, R., Rigden, A. J., Short Gianotti, D. J., Mantooth, J. A., and Templer, P. H.:  
465 Changes in autumn senescence in northern hemisphere deciduous trees: a meta-analysis of autumn phenology studies,  
466 *Ann Bot*, 116, 875–888, <https://doi.org/10.1093/aob/mcv055>, 2015.
- 467 Hufkens, K., Basler, D., Milliman, T., Melaas, E. K., and Richardson, A. D.: An integrated phenology modelling framework  
468 in R, *Methods Ecol. Evol.*, 9, 1276–1285, <https://doi.org/10.1111/2041-210x.12970>, 2018.
- 469 Inouye, D. W.: Climate change and phenology, *Wiley Interdiscip. Rev. Clim. Change*, 13, e764,  
470 <https://doi.org/10.1002/wcc.764>, 2022.
- 471 Izquierdo-Verdiguier, E., Zurita-Milla, R., Ault, T. R., and Schwartz, M. D.: Development and analysis of spring plant  
472 phenology products: 36 years of 1-km grids over the conterminous US, *Agric. For. Meteorol.*, 262, 34–41,  
473 <https://doi.org/10.1016/j.agrformet.2018.06.028>, 2018.
- 474 Jeong, S.-J. and Medvigy, D.: Macroscale prediction of autumn leaf coloration throughout the continental United States,  
475 *Global Ecol. Biogeogr.*, 23, 1245–1254, <https://doi.org/10.1111/geb.12206>, 2014.
- 476 Keenan, T. F., Gray, J., Friedl, M. A., Toomey, M., Bohrer, G., Hollinger, D. Y., Munger, J. W., O’Keefe, J., Schmid, H. P.,  
477 Wing, I. S., and others: Net carbon uptake has increased through warming-induced changes in temperate forest  
478 phenology, *Nat. Clim. Change*, 4, 598–604, <https://doi.org/10.1038/nclimate2253>, 2014.



- 479 Kowalski, K., Senf, C., Hostert, P., and Pflugmacher, D.: Characterizing spring phenology of temperate broadleaf forests  
480 using Landsat and Sentinel-2 time series, *Int. J. Appl. Earth Obs. Geoinf.*, 92, 102172,  
481 <https://doi.org/10.1016/j.jag.2020.102172>, 2020.
- 482 Lang, W., Chen, X., Qian, S., Liu, G., and Piao, S.: A new process-based model for predicting autumn phenology: how is  
483 leaf senescence controlled by photoperiod and temperature coupling?, *Agric. For. Meteorol.*, 268, 124–135,  
484 <https://doi.org/10.1016/j.agrformet.2019.01.006>, 2019.
- 485 Li, X., Zhou, Y., Meng, L., Asrar, G. R., Lu, C., and Wu, Q.: A dataset of 30 m annual vegetation phenology indicators  
486 (1985–2015) in urban areas of the conterminous United States, *Earth Syst. Sci. Data*, 11, 881–894,  
487 <https://doi.org/10.5194/essd-11-881-2019>, 2019.
- 488 Liang, L., Schwartz, M. D., and Fei, S.: Validating satellite phenology through intensive ground observation and landscape  
489 scaling in a mixed seasonal forest, *Remote Sens. Environ.*, 115, 143–157, <https://doi.org/10.1016/j.rse.2010.08.013>,  
490 2011.
- 491 Lieth, H.: *Purposes of a phenology book*, Springer, 1974.
- 492 Liu, H., Gong, P., Wang, J., Clinton, N., Bai, Y., and Liang, S.: Annual dynamics of global land cover and its long-term  
493 changes from 1982 to 2015, *Earth Syst. Sci. Data*, 12, 1217–1243, <https://doi.org/10.5194/essd-12-1217-2020>, 2020.
- 494 Liu, Q., Fu, Y. H., Zhu, Z., Liu, Y., Liu, Z., Huang, M., Janssens, I. A., and Piao, S.: Delayed autumn phenology in the  
495 Northern Hemisphere is related to change in both climate and spring phenology, *Global Change Biol.*, 22, 3702–3711,  
496 <https://doi.org/10.1111/gcb.13311>, 2016a.
- 497 Liu, Y., Wu, C., Peng, D., Xu, S., Gonsamo, A., Jassal, R. S., Arain, M. A., Lu, L., Fang, B., and Chen, J. M.: Improved  
498 modeling of land surface phenology using MODIS land surface reflectance and temperature at evergreen needleleaf  
499 forests of central North America, *Remote Sens. Environ.*, 176, 152–162, <https://doi.org/10.1016/j.rse.2016.01.021>,  
500 2016b.
- 501 Melaas, E. K., Sulla-Menashe, D., Gray, J. M., Black, T. A., Morin, T. H., Richardson, A. D., and Friedl, M. A.: Multisite  
502 analysis of land surface phenology in North American temperate and boreal deciduous forests from Landsat, *Remote  
503 Sens. Environ.*, 186, 452–464, <https://doi.org/10.1016/j.rse.2016.09.014>, 2016.
- 504 Menzel, A.: Phenology: its importance to the global change community, *Clim. Change*, 54, 379,  
505 <https://doi.org/10.1023/A:1016125215496>, 2002.
- 506 Menzel, A., Yuan, Y., Matiu, M., Sparks, T., Scheifinger, H., Gehrig, R., and Estrella, N.: Climate change fingerprints in  
507 recent European plant phenology, *Global Change Biol.*, 26, 2599–2612, <https://doi.org/10.1111/gcb.15000>, 2020.
- 508 Misra, G., Cawkwell, F., and Wingler, A.: Status of phenological research using Sentinel-2 data: A review, *Remote Sens.*,  
509 12, 2760, <https://doi.org/10.3390/rs12172760>, 2020.
- 510 Muñoz Sabater, J.: ERA5-Land hourly data from 1950 to present, Copernicus Climate Change Service (C3S) Climate Data  
511 Store (CDS) [data set], <https://doi.org/10.24381/cds.e2161bac>, 2019.



- 512 Muñoz-Sabater, J., Dutra, E., Agustí-Panareda, A., Albergel, C., Arduini, G., Balsamo, G., Boussetta, S., Choulga, M.,  
513 Harrigan, S., Hersbach, H., and others: ERA5-Land: A state-of-the-art global reanalysis dataset for land applications,  
514 Earth Syst. Sci. Data, 13, 4349–4383, <https://doi.org/10.5194/essd-13-4349-2021>, 2021.
- 515 Nasahara, K. N. and Nagai, S.: Development of an in situ observation network for terrestrial ecological remote sensing: the  
516 Phenological Eyes Network (PEN), Ecol. Res., 30, 211–223, <https://doi.org/10.1007/s11284-014-1239-x>, 2015.
- 517 Park, D. S., Newman, E. A., and Breckheimer, I. K.: Scale gaps in landscape phenology: challenges and opportunities,  
518 Trends Ecol. Evol., 36, 709–721, <https://doi.org/10.1016/j.tree.2021.04.008>, 2021.
- 519 Peng, D., Wu, C., Li, C., Zhang, X., Liu, Z., Ye, H., Luo, S., Liu, X., Hu, Y., and Fang, B.: Spring green-up phenology  
520 products derived from MODIS NDVI and EVI: Intercomparison, interpretation and validation using National Phenology  
521 Network and AmeriFlux observations, Ecol. Indic., 77, 323–336, <https://doi.org/10.1016/j.ecolind.2017.02.024>, 2017.
- 522 Phillips, S. J., Anderson, R. P., and Schapire, R. E.: Maximum entropy modeling of species geographic distributions, Ecol.  
523 Modell., 190, 231–259, <https://doi.org/10.1016/j.ecolmodel.2005.03.026>, 2006.
- 524 Piao, S., Liu, Q., Chen, A., Janssens, I. A., Fu, Y., Dai, J., Liu, L., Lian, X., Shen, M., and Zhu, X.: Plant phenology and  
525 global climate change: Current progresses and challenges, Glob Chang Biol, 25, 1922–1940,  
526 <https://doi.org/10.1111/gcb.14619>, 2019.
- 527 Polgar, C. A. and Primack, R. B.: Leaf-out phenology of temperate woody plants: from trees to ecosystems, New Phytol.,  
528 191, 926–941, <https://doi.org/10.1111/j.1469-8137.2011.03803.x>, 2011.
- 529 Richardson, A. D., Keenan, T. F., Migliavacca, M., Ryu, Y., Sonnentag, O., and Toomey, M.: Climate change, phenology,  
530 and phenological control of vegetation feedbacks to the climate system, Agric. For. Meteorol., 169, 156–173,  
531 <https://doi.org/10.1016/j.agrformet.2012.09.012>, 2013.
- 532 Richardson, A. D., Hufkens, K., Milliman, T., Aubrecht, D. M., Chen, M., Gray, J. M., Johnston, M. R., Keenan, T. F.,  
533 Klosterman, S. T., Kosmala, M., and others: Tracking vegetation phenology across diverse North American biomes  
534 using PhenoCam imagery, Sci. Data, 5, 1–24, <https://doi.org/10.1038/sdata.2018.28>, 2018.
- 535 Rodriguez-Galiano, V., Dash, J., and Atkinson, P. M.: Intercomparison of satellite sensor land surface phenology and ground  
536 phenology in Europe, Geophys. Res. Lett., 42, 2253–2260, <https://doi.org/10.1002/2015gl063586>, 2015.
- 537 Schwartz, M. D.: Phenology: an integrative environmental science, Springer, 2003.
- 538 Schwartz, M. D., Betancourt, J. L., and Weltzin, J. F.: From Caprio’s lilacs to the USA national phenology network, Front.  
539 Ecol. Environ., 10, 324–327, <https://doi.org/10.1890/110281>, 2012.
- 540 Schwartz, M. D., Ault, T. R., and Betancourt, J. L.: Spring onset variations and trends in the continental United States: past  
541 and regional assessment using temperature-based indices, Int. J. Climatol., 33, 2917–2922,  
542 <https://doi.org/10.1002/joc.3625>, 2013.
- 543 Studer, S., Stöckli, R., Appenzeller, C., and Vidale, P. L.: A comparative study of satellite and ground-based phenology, Int.  
544 J. Biometeorol., 51, 405–414, <https://doi.org/10.1007/s00484-006-0080-5>, 2007.



- 545 Tang, J., Körner, C., Muraoka, H., Piao, S., Shen, M., Thackeray, S. J., and Yang, X.: Emerging opportunities and  
546 challenges in phenology: a review, *Ecosphere*, 7, e01436, <https://doi.org/10.1002/ecs2.1436>, 2016.
- 547 Tao, Z., Wang, H., Dai, J., Alatalo, J., and Ge, Q.: Modeling spatiotemporal variations in leaf coloring date of three tree  
548 species across China, *Agric. For. Meteorol.*, 249, 310–318, <https://doi.org/10.1016/j.agrformet.2017.10.034>, 2018.
- 549 Templ, B., Koch, E., Bolmgren, K., Ungersböck, M., Paul, A., Scheifinger, H., Rutishauser, T., Busto, M., Chmielewski, F.-  
550 M., Hájková, L., and others: Pan European Phenological database (PEP725): a single point of access for European data,  
551 *Int. J. Biometeorol.*, 62, 1109–1113, <https://doi.org/10.1007/s00484-018-1512-8>, 2018.
- 552 Tian, F., Cai, Z., Jin, H., Hufkens, K., Scheifinger, H., Tagesson, T., Smets, B., Van Hoolst, R., Bonte, K., Ivits, E., and  
553 others: Calibrating vegetation phenology from Sentinel-2 using eddy covariance, PhenoCam, and PEP725 networks  
554 across Europe, *Remote Sens. Environ.*, 260, 112456, <https://doi.org/10.1016/j.rse.2021.112456>, 2021.
- 555 Wang, H., Dai, J., and Ge, Q.: The spatiotemporal characteristics of spring phenophase changes of *Fraxinus chinensis* in  
556 China from 1952 to 2007, *Sci. China Earth Sci.*, 55, 991–1000, <https://doi.org/10.1007/s11430-011-4349-0>, 2012.
- 557 Wang, H., Ge, Q., Rutishauser, T., Dai, Y., and Dai, J.: Parameterization of temperature sensitivity of spring phenology and  
558 its application in explaining diverse phenological responses to temperature change, *Sci. Rep.*, 5, 8833,  
559 <https://doi.org/10.1038/srep08833>, 2015.
- 560 Wang, H., Wu, C., Ciais, P., Peñuelas, J., Dai, J., Fu, Y., and Ge, Q.: Overestimation of the effect of climatic warming on  
561 spring phenology due to misrepresentation of chilling, *Nat. Commun.*, 11, 4945, [https://doi.org/10.1038/s41467-020-](https://doi.org/10.1038/s41467-020-18743-8)  
562 18743-8, 2020a.
- 563 Wang, L., Tian, F., Huang, K., Wang, Y., Wu, Z., and Fensholt, R.: Asymmetric patterns and temporal changes in  
564 phenology-based seasonal gross carbon uptake of global terrestrial ecosystems, *Global Ecol. Biogeogr.*, 29, 1020–1033,  
565 <https://doi.org/10.1111/geb.13084>, 2020b.
- 566 Wu, C., Hou, X., Peng, D., Gonsamo, A., and Xu, S.: Land surface phenology of China's temperate ecosystems over 1999–  
567 2013: Spatial–temporal patterns, interaction effects, covariation with climate and implications for productivity,  
568 *Agricultural and Forest Meteorology*, 216, 177–187, <https://doi.org/10.1016/j.agrformet.2015.10.015>, 2016.
- 569 Wu, C., Wang, X., Wang, H., Ciais, P., Peñuelas, J., Myneni, R. B., Desai, A. R., Gough, C. M., Gonsamo, A., Black, A. T.,  
570 and others: Contrasting responses of autumn-leaf senescence to daytime and night-time warming, *Nat. Clim. Change*, 8,  
571 1092–1096, <https://doi.org/10.1038/s41558-018-0346-z>, 2018.
- 572 Wu, W., Sun, Y., Xiao, K., and Xin, Q.: Development of a global annual land surface phenology dataset for 1982–2018 from  
573 the AVHRR data by implementing multiple phenology retrieving methods, *Int. J. Appl. Earth Obs. Geoinf.*, 103,  
574 102487, <https://doi.org/10.1016/j.jag.2021.102487>, 2021a.
- 575 Wu, Z., Chen, S., De Boeck, H. J., Stenseth, N. C., Tang, J., Vitasse, Y., Wang, S., Zohner, C., and Fu, Y. H.: Atmospheric  
576 brightening counteracts warming-induced delays in autumn phenology of temperate trees in Europe, *Global Ecol.*  
577 *Biogeogr.*, 30, 2477–2487, <https://doi.org/10.1111/geb.13404>, 2021b.



- 578 Ye, Y., Zhang, X., Shen, Y., Wang, J., Crimmins, T., and Scheifinger, H.: An optimal method for validating satellite-derived  
579 land surface phenology using in-situ observations from national phenology networks, *ISPRS J. Photogramm. Remote*  
580 *Sens.*, 194, 74–90, <https://doi.org/10.1016/j.isprsjprs.2022.09.018>, 2022.
- 581 Zani, D., Crowther, T. W., Mo, L., Renner, S. S., and Zohner, C. M.: Increased growing-season productivity drives earlier  
582 autumn leaf senescence in temperate trees, *Science*, 370, 1066–1071, <https://doi.org/10.1126/science.abd8911>, 2020.
- 583 Zhang, X., Wang, J., Gao, F., Liu, Y., Schaaf, C., Friedl, M., Yu, Y., Jayavelu, S., Gray, J., Liu, L., and others: Exploration  
584 of scaling effects on coarse resolution land surface phenology, *Remote Sens. Environ.*, 190, 318–330,  
585 <https://doi.org/10.1016/j.rse.2017.01.001>, 2017.
- 586 Zhang, X., Wang, J., Henebry, G. M., and Gao, F.: Development and evaluation of a new algorithm for detecting 30 m land  
587 surface phenology from VIIRS and HLS time series, *ISPRS J. Photogramm. Remote Sens.*, 161, 37–51,  
588 <https://doi.org/10.1016/j.isprsjprs.2020.01.012>, 2020a.
- 589 Zhang, X., Friedl, M., and Henebry, G.: VIIRS/NPP Land Cover Dynamics Yearly L3 Global 0.05 Deg CMG V001, NASA  
590 EOSDIS Land Processes DAAC, accessed on 2022-08-11, <https://doi.org/10.5067/VIIRS/VNP22C2.001>, 2020b.
- 591 Zhu, M., Dai J.: Species phenology and ground phenology maps over China from 1951-2020, *Science Data Bank [data set]*,  
592 <https://doi.org/10.57760/sciencedb.07995>. DOI:10.57760/sciencedb.07995, 2023.